



## VERIFICATION OF EFFECTS BASED ON FULL-SCALE WOODEN FRAME TESTS WITH ARAMID FIBER SHEET REINFORCEMENT TITLE

T. Ogino<sup>(1)</sup>, Y. Asaoka<sup>(2)</sup>, S. Koike<sup>(3)</sup>, A. Yamaguchi<sup>(4)</sup>, X. Chen<sup>(5)</sup>, N. Takiyama<sup>(6)</sup>

<sup>(1)</sup> Undergraduate, Tokyo Metropolitan University, tomotomo19980227@gmail.com

<sup>(2)</sup> A one-time Undergraduate, Tokyo Metropolitan University, qiezi987654321@gmail.com

<sup>(3)</sup> Graduate, Tokyo Metropolitan University, abcdefghi123456789@icloud.com

<sup>(4)</sup> A one-time Graduate, Tokyo Metropolitan University, toteaakari@gmail.com

<sup>(5)</sup> Graduate, Tokyo Metropolitan University, overloadedlife@gmail.com

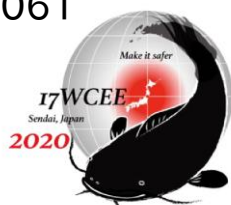
<sup>(6)</sup> Associate Professor, Tokyo Metropolitan University, norikot@tmu.ac.jp

### Abstract

Aramid fiber is a new type of high-performance fiber made up of polyamide. It can be made into aramid fiber sheets through braiding. One of the conventional methods for reinforcing wooden frame joints is to use an aramid fiber sheet. Because this reinforcement method only affixes a sheet by adhering it to the joint, it is easy to use, and large-scale construction is rendered unnecessary. We aim to further develop this method by increasing the reinforcement effect. In a previous study, we investigated column bases that were bent and pulled out during an earthquake and performed static bending and pull-out tests on column base joints reinforced with aramid fiber sheets to verify the relationship between sheet affixing type, fracture properties, and restoring force characteristics. Various destructive properties occurred, and brittle fractures were suppressed when the sheet was split in the fiber direction and had a destructive property of sequentially peeling from the outer edge. Therefore, it was confirmed that the bending deformation performance can be improved by constructing the sheet in advance in a split shape and artificially manipulating the destructive properties.

Based on those findings, in this study we have two objectives: (a) perform additional static bending tests of column base joints to understand the change in restoring force due to the split type and (b) perform a static loading full-scale frame test and confirm the relationship between the deformation of the actual frame where the column axial force acts on it and the joint damage.

**Keywords:** *New material, restoring force characteristics, deformation performance, destructive properties*



## 1. Introduction

With past earthquakes, there were many cases of collapsed wooden houses due to joint damage. In Japan, the revision of the Building Standards Law in 2000 [1] stipulated that wooden joints were to be reinforced with metal. This reinforcement, which incurs a section loss, has been put to practical use in reinforced concrete buildings in recent years, but there are many unconfirmed items regarding earthquake resistance in relation to wooden buildings.

The authors are conducting a series of studies aimed at developing more effective reinforcement methods. In previous research, we focused on column bases that are subject to bending and pulling out during earthquakes [2] [3].

In previous studies, pull-out tests and bending tests were performed on column-base joints reinforced with aramid fiber sheets, and the relationship between the sheet attachment format and mechanical properties was systematically verified. The following results were found: (a) the reinforced resin plastic layer crushed when subjected to a compressive force, and the problem was solved by providing a resin to a non-impregnated area in a portion of the column to be subjected to the compressive force [4]. (b) During column bending and deformation, if the diagonally affixed sheet tears in a split shape and peels off sequentially from the outer edge, the brittle destruction is suppressed, and the sheet is pre-constructed in the split shape and destroyed. We proposed a method to control the properties and improve the deformation performance [5].

Based on the above findings, this study aims to further improve the bending deformation performance and proposes a reinforcement method. Additionally, the static loading test of the reinforced full-scale wooden frame structure verifies the behavior of the aramid fiber sheet damage and earthquake. Regarding the vertical application, verification is performed by changing to a polyethylene terephthalate (PET) woven sheet to improve the deformation performance of the sheet against tension.

## 2. About the sheet

### 2.1 Aramid fiber sheet and its construction method [6]

The aramid fiber sheet is composed of a fiber bundle where one aramid fiber has a thickness of several  $\mu\text{m}$  and is bundled in one or two directions in a unit of several hundred to thousands. Three fiber bundles are defined as one ridge. One ridge has approximately seven times the tensile strength of steel, is approximately one fifth of the weight, has high strength, and is lightweight. It is also flexible, non-conductive, non-magnetic, highly durable, and resistant to impact.

The aramid fiber sheet method involves a sheet being impregnated with a resin and attached to a structural material to form a reinforced plastic layer (AFRP) to improve the proof stress of the structure and prevent deterioration.

### 2.2 PET sheet [7]

The PET sheet is made of a PET fiber sheet that is woven with an irregular woven pattern and has excellent resin impregnation properties. Table 1 illustrates that the elongation at the break is larger than that of the aramid fiber sheet.

Seven 1670dtex filament yarns are plied, and two of them are drawn together to form one bundle. Three bundles of filament yarn constitute one ridge, and there are 51 ridges.

In addition, if the sheet is cut into a split shape, the fibers will unravel. Therefore, in this study, a fray prevention seal is attached to both ends of one surface of the sheet.



Fig. 1 Aramid fiber sheet.



Fig. 2 PET sheet.



Table 1 – Specifications of sheet mosaic weave

Type	Product number	Design thickness mm	Tensile strength N/mm <sup>2</sup>	Elastic modulus kN/mm <sup>2</sup>	Elongation at break %
PET Sheet	PET-600	0.906	740	10±1	7% or greater
Aramid Fiber Sheet	AK-600	0.286	2,100	118±15	1.8

### 3. Bending test of inverted T-shaped specimen

#### 3.1 Overview of test specimen

Figure 3 shows the outline of the test specimen. The cedar wood 105 mm square pillar and base are short tenoned in a reverse T-shape and fastened with V-shaped hardware. To simulate aramid fiber sheet reinforcement for joints with a history of damage, they are applied once and then damaged. Afterwards, the V-shaped hardware is removed, reinforced with aramid fiber sheets, and re-forced based on standard practice.

Table 2 displays the sheet attachment format. In this study, some sheets are divided in advance into splits. Silicone resin is used for the area 10 mm above and below the joint where the adhesive is not applied (hereinafter referred to as the non-impregnated area), and for the triangular area where the sheet and wood are not bonded (hereinafter referred to as the wood non-bonded area).

A description is provided for the specimen which has a name beginning with “T.” In the figure, the number following the T indicates the specimen number. Specimens marked with a “P” use PET sheets for the vertical application. Additionally, “s” indicates the silicon resin impregnation into the non-impregnated area and wood non-bonded portion. “h” indicates a PET sheet with a non-fray seal that is left between the wood and the sheet; h indicates a one-sided sheet and hh indicates a double-sided sheet.

Other test pieces are also described. PCS1 and PCS2 are improved forms of the precast proposed in previous research. Specimen PCS1 has a vertical attachment of 500 mm + 45° cross-attachment, while specimen PCS2 has a vertical attachment of 400 mm + 60° cross-attachment. Specimens AS1 and AS2 are improved types where precast types PC1 and PC2 are made into short fences. The specimen AS3 uses the same affixing method as that of the reinforcing method of the frame specimen described later on. Additionally, the sheet is double-sided for all the test pieces, and the length of the vertical sheet equalizes the bonding area between the pillar and the base when adjusting the position of the cross-sheet. Table 3 shows the specifications of the aramid fiber sheet, PET sheet, epoxy resin, and silicone resin.

Table 2 – Sheet type of test specimen and test results

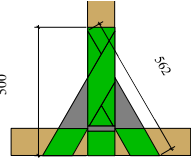
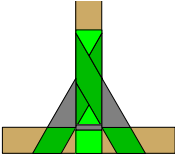
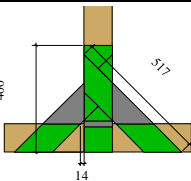
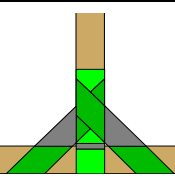
1 <sup>st</sup> force application	2 <sup>nd</sup> force application	3 <sup>rd</sup> force application
 <p>T1s <math>F_{max}</math>:6.00kN (1/15rad)</p>	 <p>TP1s <math>F_{max}</math>:5.50kN (1/15rad)</p>	
 <p>T2s <math>F_{max}</math>:7.70kN (1/10rad)</p>	 <p>TP2s <math>F_{max}</math>:6.90kN (1/10rad)</p>	



Table 2 – Sheet type of test specimen and test results - continued

<p>T3s <math>F_{max}</math>:4.50kN (1/10rad)</p>	<p>TP3shh <math>F_{max}</math>:3.60kN (1/15rad)</p>	<p>TP3s <math>F_{max}</math>:4.10kN (1/15rad)</p>
<p>T4s <math>F_{max}</math>:6.20kN (1/10rad)</p>	<p>TP4sh <math>F_{max}</math>:3.50kN (1/10rad)</p>	<p>TP4s <math>F_{max}</math>:7.80kN (1/10rad)</p>
<p>T5 <math>F_{max}</math>:5.50kN (1/15rad)</p>	<p>TP5sh <math>F_{max}</math>:3.20kN (1/15rad)</p>	<p>TP5s <math>F_{max}</math>:6.20kN (1/10rad)</p>
<p>PCS1 <math>F_{max}</math>:6.74kN(1/10rad)</p>	<p>AS1 <math>F_{max}</math>:5.64kN (1/15rad)</p>	
<p>PCS2 <math>F_{max}</math>:3.44kN (1/15rad)</p>	<p>AS2 <math>F_{max}</math>:2.75kN (1/20rad)</p>	
<p>AS3 <math>F_{max}</math>:4.81kN (1/15rad)</p>		



### 3.2 Test method

Figure 4 illustrates the force applying device. The test specimen base is fastened to the base of the loading device with anchor bolts. The front side of the drawing is called the S side, and the back side is called the N side. For the applied force, the jig of the actuator is connected to the specimen with a stroke of 300 mm. The value obtained by dividing the measured value of the wire displacement meter installed at the top of the test piece column by the column height is defined as the test piece deformation angle, and the alternating positive and negative forces are repeated twice from approximately 1/120 rad to 1/5 rad. In addition, the rotation angle of the joint is calculated by a contact displacement meter.

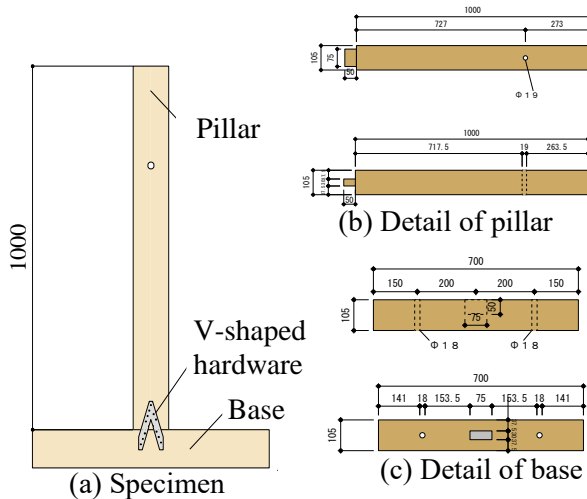


Fig.3 Detail of the specimen.

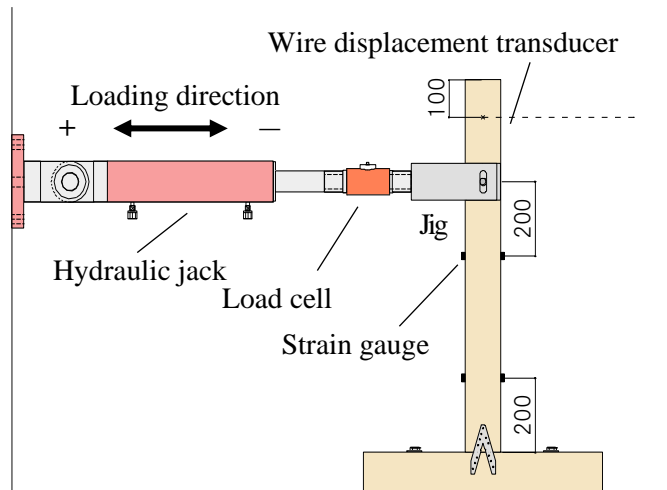


Fig.4 Loading system (south side).

Table 3 –Material specifications

Aramid Fiber Sheet	Product name: FiBRA Sheet AK-40、 Width: 100 mm Tensile strength: 2,060 N/mm <sup>2</sup> 、 Young's modulus: 118 kN/mm <sup>2</sup> Design thickness: 0.193 mm、 Manufacturer: Fibex Co., Ltd.
PET Sheet	Product name: PET Sheet 600-30、 Width: 100 mm Tensile strength: 740 N/mm <sup>2</sup> 、 Young's modulus: 10 kN/mm <sup>2</sup> Design thickness: 0.906 mm、 Manufacturer: Fibex Co., Ltd.
Bonding epoxy resin impregnation	Product name: Asahi bond, 701 [8] Tensile strength: 38.3 N/mm <sup>2</sup> 、 Bending strength: 66.0 N/mm <sup>2</sup> Manufacturer: Asahi Bond, Inc.
Silicone resin	Product name: Silicone sealant Cemedine, 8051N Manufacturer: Cemedine, Inc.

### 3.3 Experiment results

Table 2 shows the maximum horizontal resistance  $F_{\max}$  (kN) and its deformation angle (rad). Based on Table 2, the test specimen with the highest maximum horizontal resistance and deformation angle was TP4s in the split state and T2s in the single-sheet application.



## 4. Static loading test of frame specimen

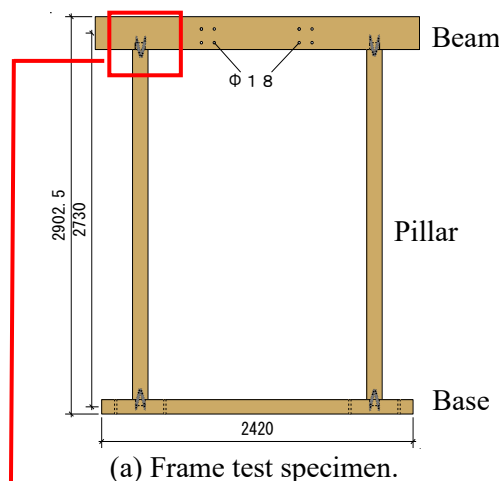
### 4.1 Specimen overview

Figure 5 displays the outline of the test specimen. Cedar wood is used for the girder, pillar, and base, and short tenon joints are made. Considering the analysis model [2] from the previous research study, the number of ridges on the sheet is vertically applied at a ratio of 12:7:12, and the cross applied is divided into a ratio of 7:8:7:8 from the outer edge, and they are applied to both sides. Silicon is impregnated into the joint interface of the member and non-bonded portion of the wood.

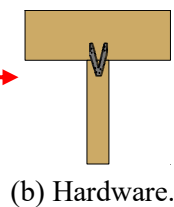
### 4.2 Loading/measurement method

The base is fixed to the steel frame with anchor bolts, and the load is 1 t per pillar. A positive/negative alternating incremental repetitive force is applied via a jig installed on the top of the test body. The force direction is positive when it faces left on the paper. The positive column is a W column, and the negative column is an E column. Additionally, the S side is on the front side, and the N side is on the back side.

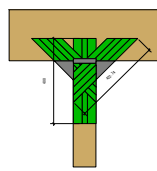
A load cell is installed on the top, the horizontal resistance of the specimen is measured, and the absolute displacement is measured using a wire displacement meter. The value obtained by dividing the absolute displacement by the inner height of the column is defined as the interlayer deformation angle  $R$ . The force is applied twice based on the amplitude of  $R$  from  $1/120$  rad to  $1/5$  rad, and the applied force direction is positive in the left direction of the paper. the force is applied until the maximum deformation angle  $\pm 1/5$  rad or horizontal resistance is lost [9] [10].



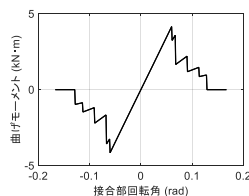
(a) Frame test specimen.



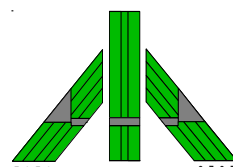
(b) Hardware.



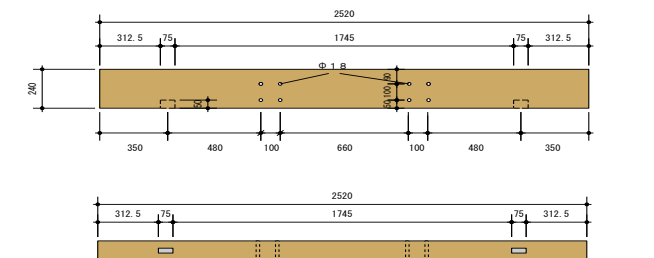
(c) Sheet.



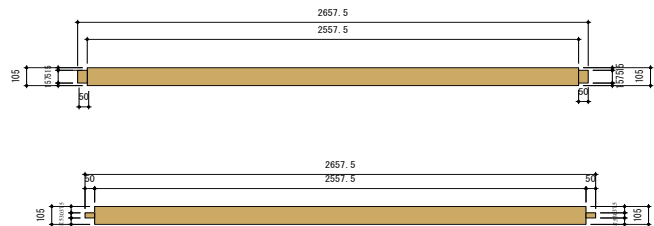
(d) Analysis value.



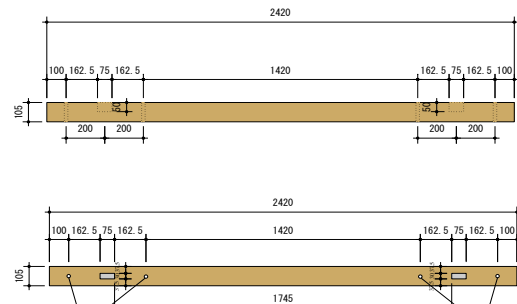
(e) Sheet division number.



(f) Beam detail.



(g) Pillar detail.



(h) Base detail.

Fig. 5 Outline of the frame specimen and sheet division method.





### 4.3 Experiment results

Photo 1 illustrates the main fracture properties, and Fig. 6 shows the relationship between the horizontal load and interlayer deformation angle.

With the V-shaped hardware, the tenon of the column base of the E column began to split at an interlayer deformation angle of  $1/6$  rad. At  $1/5$  rad, the column base was entrapped, and the tenon of the W column base split. At  $1/75$  rad, the maximum horizontal resistance was  $0.57$  kN, and at  $1/5$  rad, the applied force was terminated.

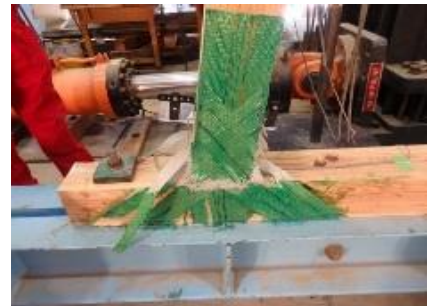
With the after sheet reinforcement, the split aramid fiber sheet was peeled off in order beginning with the outer edge on all surfaces. At  $1/20$  rad, it began to peel off, and at  $1/10$  rad the cross stuck on the capital of the W was nearly fully peeled off. At  $1/8$  rad, cross-bonding of other joints began to peel off from the outside, and at  $1/6$  rad all N-side vertical sticks of the E column bases peeled off from the column. However, sheets at other joints peeled off from the base side. The maximum horizontal resistance was  $3.17$  kN at  $1/15$  rad, and the horizontal resistance was lost at  $1/6$  rad when the sheet was nearly peeled off, and the loading was terminated.



(a) Experiment at  $1/6$  rad.



(b) Splitting the specimen at  $1/8$  rad.



(c) Western capital at  $-1/6$  rad.



(d) Western pedestal at  $1/6$  rad.

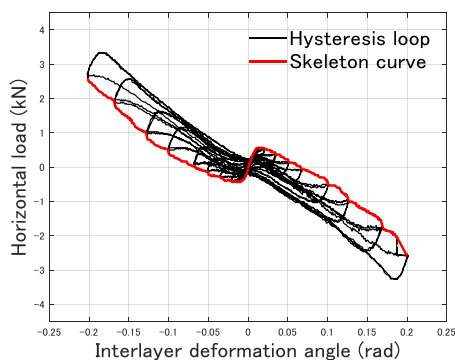


(e) East capital at  $-1/6$  rad.

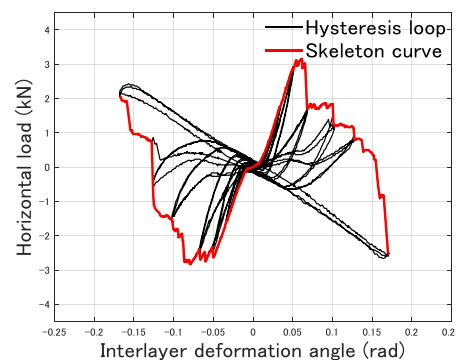


(f) East pedestal at  $-1/6$  rad.

Photo 1 Major destruction.



(a) V-shaped hardware.



(b) Sheet reinforcement.

Fig. 6 Relationship between horizontal load and interlayer deformation angle.



## 5. Consideration

### 5.1 Comparison of restoring force characteristics and fracture properties of static bending test

Figure 7 illustrates the relationship between the bending moment  $M$  of the column and the joint rotation angle  $\theta$  as the restoring force characteristic. In addition, the compared skeletal curves are drawn in an overlapping manner. The results are discussed below.

(1) The T1s, T2s, PCS1, and PCS2 formats of the bCS45<sup>A</sup> format (reported previously) [4] are compared with changed cross-sticking angles and lengths (Fig. 7(a)). The maximum strength is higher when the cloth is pasted at 45° than it is at 60°, and it is higher when the cross-pasting interval increases. The relative deformation performance is as follows: bCS45<sup>A</sup> > PCS1 > T2s > T1s > PCS2.

(2) T4s, TP4s, and AS1 (with a PCS1 that has the same attachment format but different vertical attachment and ridge division numbers) are compared (Fig. 7(b)). TP4s has the maximum proof stress, but the relative deformation performance was in the following order: AS1 > PCS1 > TP4s > T4s. For the number of ridge divisions of the cloth attachment, if the ridges are attached in descending order from the outer edge, then the deformation performance is high. Additionally, bCS45<sup>A</sup> is compared with T3s, TP3s, and AS3 (Fig. 7(c)). Although the maximum resistance is nearly equal, the relative deformation performance is as follows: TP3s > bCS45<sup>A</sup> > T3s > AS3. Because the base of TP3s splits before the maximum yield strength, the maximum yield strength is estimated to be higher than the experimental value.

(3) Comparing T3s with TP3shh and TP3s, which differ only in the vertical sheet format (Fig. 7(d)), TP3s had the highest deformation performance, and T3s had the highest maximum resistance. In addition, they are compared based on the presence or absence of a fray prevention seal. Comparing TP3shh and TP3s of the PET sheet with the vertical application, TP3s had higher maximum resistance and deformation performance.

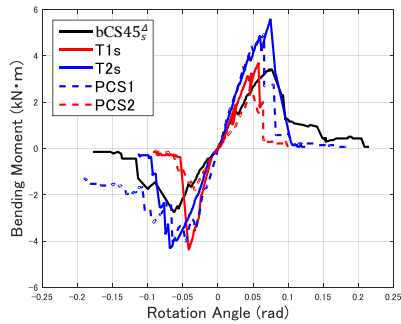
(4) The cases where the sticking format is the same and the base material is different are compared (Fig. 7(e)). The base of T5 is bay pine, and the base of AS3 is cedar. The maximum resistance was higher for T5, but the deformation performance was higher for AS3. It is postulated that compression crushing occurred for T5 because part of the resin dripped at the column base interface during construction.

(5) A comparison is made for the attachment format adopted for the frame test specimen (AS3 and T3s in this report) (Fig. 7(f)). On the negative side, T3s is high in both maximum resistance and deformation performance, causing gradual destruction.

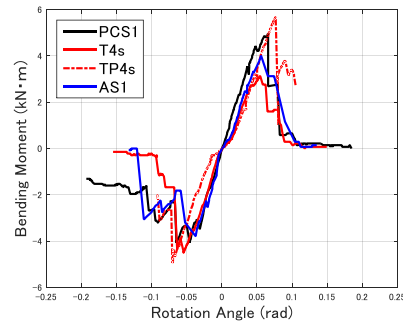
(6) The experimental value of T3s and the analysis value are compared (Fig. 7 (g)). The initial stiffness was nearly the same on both the positive and negative sides. On the negative side, the resistance was lost at nearly the same timing in the skeletal curve for the experimental and analytical values. On the positive side of the experimental values, the resistance was likely largely lost because a plurality of cross-bonded sheets peeled off at the joint rotation angle of 0.07 rad.

(7) A comparison between the experimental and analytical values of T5 using bay pine as the base is performed (Fig. 7 (h)). The initial stiffness was nearly the same on both the positive and negative sides. On the positive side, the analytical value of the maximum proof stress was higher, but the joint rotation angle at the maximum proof stress was nearly the same value. The experimental value was due to the resin dripping in the non-impregnated range, and a compression failure occurred in that range. As a result, the split breaking of the sheet was stopped only at part of the outer edge of the cloth attachment, and the stepwise breaking as with the analysis value did not occur.

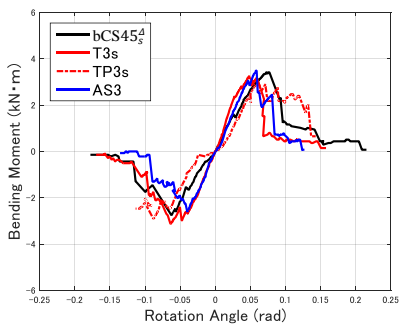




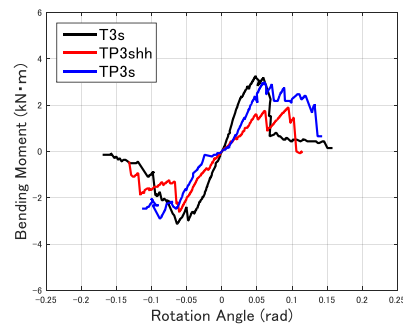
(a) Comparison of single-stick format.



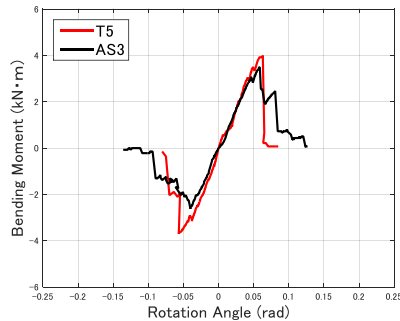
(b) Comparison of cross pasting 45° outside format.



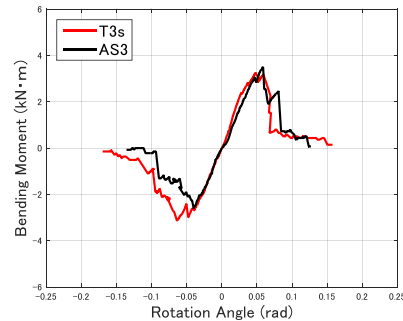
(c) Comparison of cross pasting 45° center format.



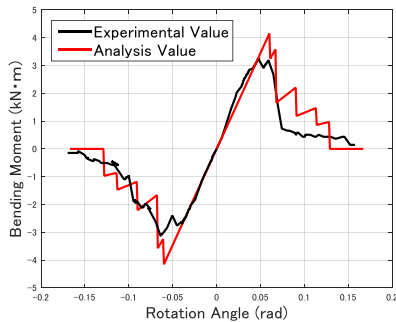
(d) Comparison of sheet attachment types.



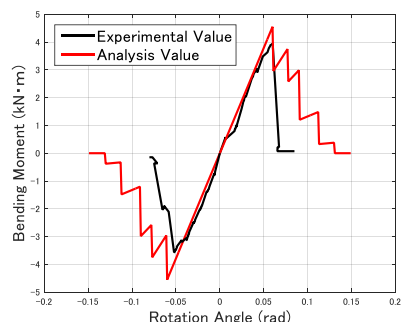
(e) Comparison of base material types.



(f) Type comparison of frame test



(g) Comparison of analysis value 1.



(h) Comparison of analysis value 2.

Fig. 7 Relationship between bending moment  $M$  and joint rotation angle  $\theta$ .



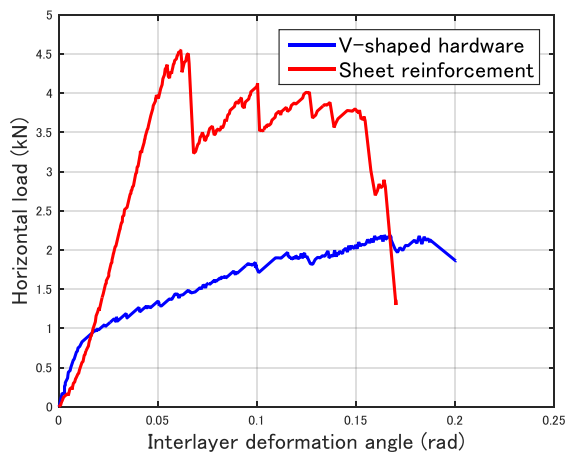
## 5.2 Comparison of static loading experiments

### 5.2.1 Comparison of V-shaped hardware and sheet reinforcement

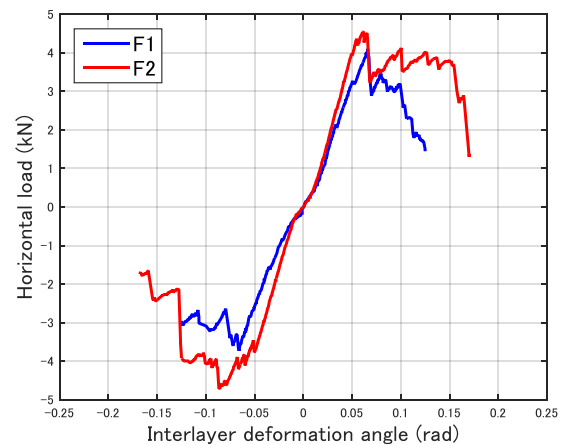
Figure 8 (a) displays a comparison of the skeletal curves with the  $P\Delta$  effect that are removed from the relationship between the horizontal load and the interlayer deformation angle. After sheet reinforcement, the maximum proof stress is twice as large as that of the V-shaped metal; the deformation performance was not significantly inferior to that of the V-shaped metal, and brittle fractures were avoided.

### 5.2.2 Comparison with previous studies

The frame test specimen previously reported is F1[5], the test specimen of this report is F2, and the horizontal load-interlaminar deformation angle relationship is compared in Fig. 8 (b). Both the maximum horizontal resistance and the deformation performance were higher for F2. Gradual destruction is seen for F2 on both the positive and negative sides.



(a) Comparison of V-shaped hardware and sheet reinforcement.

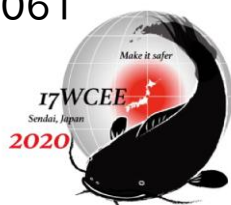


(b) Comparison with F1.

Fig. 8 Relationship between horizontal load and interlayer deformation angle.

## 6. Conclusion

This study aimed to improve the bending deformation performance of column-base joints reinforced with aramid fiber sheets, and further improvement proposals such as a reinforcement method using PET sheets were made. In addition, the damage of the aramid fiber sheet and behavior at the time of the earthquake were verified by comparing the static loading test of the reinforced full-scale wooden frame structure with that of previous research.



## 7. Acknowledgments

This research was supported by Grants-in-Aid for Scientific Research (C) NO.17K06649 (representative: Noriko Takiyama), the Obayashi Foundation Research Grant for FY2016 (representative: Noriko Takiyama), and the Maeda Memorial Engineering Promotion Foundation. This study was performed under the auspices of a research grant (representative: Noriko Takiyama) in FY2018. Fibex Co., Ltd. provided the aramid fiber sheet and Asahi Bond Industry Co., Ltd. provided the resin for this experiment.

## 8. References

- [1] Ministry of Land, Infrastructure, Transport and Tourism Retrieved from <http://www.mlit.go.jp/index.html>, on January 1, 2019 (in Japanese).
- [2] Tezuka J, Noguchi T, Yamashita J, Taniguchi H (2003): Test and evaluation of wooden pedestal using aramid fiber sheet and metal fittings (combined use), *Abstracts of Architectural Institute of Japan*, C-1, Structure I, pp.13-14, Japan.
- [3] Tezuka J, Noguchi T, Yamashita J, Taniguchi H (2004): Test report of column base of wooden structure using aramid fiber sheet and evaluation for practical use, *Abstracts of Architectural Institute of Japan*, C-1, Structure III, pp.385-386.
- [4] Yamaguchi A, Koike S, Chen X, Takiyama N (2018): Systematic verification experiment of aramid fiber sheet pasting style for column reinforcement of existing wooden buildings, *Architectural Institute of Japan Kanto Chapter Research Report*, Japan.
- [5] Asaoka Y, Koike S, Chen X, Takiyama N (2019): Improvement of deformation performance of pillar-base joint of wooden houses with aramid fiber sheet reinforcement method, *Journal of Architectural Institute of Japan*, Kanto Chapter, Japan.
- [6] Fibex Co., Ltd. Retrieved from <http://www.fibex.co.jp/index.html> on December 25, 2019 (in Japanese).
- [7] Nakai H, Sato H, Anggawidjaja D, Ueda T (2005): Seismic retrofit by continuous fiber sheet with large fracturing strain, Japan.
- [8] Asahi Bond, Inc. Retrieved from <http://www.asahibond.co.jp/> on January 1, 2019 (in Japanese).
- [9] Idate N, Takiyama N (2015): Influence of Seismic Element Arrangement of Traditional Wooden Buildings on Mechanical Properties: Part 1. Static Loading Test of Plane Frames with Large Cross Sections, *Architectural Institute of Japan Kanto Chapter Research Reports*, Vol. 85, No. I, pp. 309-312.
- [10] Idate N, Takiyama N (2016): Effects of the seismic element arrangement of traditional wooden buildings on mechanical properties: Part 2. Static loading test of two-span plane frames with different element arrangements, *Architectural Institute of Japan Kanto Chapter Research Reports*, Vol 86, Issue I, pp. 357-360, Japan.